South African Journal for Science and Technology
ISSN: (Online) 2222-4173, (Print) 0254-3486

Substituent and isomeric effects on the reduction and oxidation potential of tris(β-diketonato) manganese (III) complexes: DFT and MESP analysis

Authors:
Adebayo A. Adeniyi* [a,c], Jeanet Conradie* [b,c]

Affiliations:
[a] Department of Industrial Chemistry, Federal University Oye Ekiti, Nigeria
[b] Department of Chemistry, University of Tromsø, N-9037 Tromsø, Norway
[c] Department of Chemistry, University of the Free State, PO Box 339, Bloemfontein, 9300, South Africa

Corresponding authors:
Adebayo A. Adeniyi
E-mail: AdeniyiAA@ufs.ac.za
J. Conradie
E-mail: conradj@ufs.ac.za

Dates:
Received: 30/04/19
Accepted: 20/08/19
Published:

How to cite this article:
Adebayo A. Adeniyi, Jeanet Conradie, Substituent and isomeric effects on the reduction and oxidation potential of tris(β-diketonato) manganese (III) complexes: DFT and MESP analysis, *Suid-Afrikaanse Tydskrif vir Natuurwetenskap en Tegnologie* 38(1) (2019)

'n Afrikaanse vertaling van die manuskrip is aanlyn beskikbaar by http://www.satnt.ac.za/index.php/satnt/article/view/728

The reduction of tris(β-diketonato)manganese(III) ([Mn(β-diketonato)$_3$]) derivatives to tris(β-diketonato)manganese(II) and their oxidation to tris(β-diketonato)manganese(IV) was studied using DFT methods. The accuracy of prediction of the reduction potential or oxidation potential is very significant for their customized design, for determining the range of potentials that will be suitable for specific desired applications. The DFT functional method M06 reproduced the experimental reduction potential to a higher level of accuracy compared to M062X and B3LYP. The study also showed that the reduction of the molecules resulted in a decrease in the entropy and the Gibbs free energy of both the gas phase and the solvent phase, consequently yielding the highest value of total Gibbs free energy of reaction (ΔG_{rxt}) for the reduced molecule, especially for those molecules containing stronger electron withdrawing groups like CF_3. This led to the shifting of the reduction potential of the molecules containing CF_3 to more positive values. The more positive the reduction potential of the molecules became in the presence of stronger electron withdrawing groups, the more positive their oxidation potential shifted. This consequently rendered the oxidation potential impossible to be observed within the experimental solvent window. The values of the molecular electrostatic surface potential (MESP) minima and MESP atomic potential of Mn and coordinating oxygen atoms, served as good descriptors for the observed experimental reduction potential and might also assist in predicting the experimental reduction of further molecules to a high level of accuracy.

Keywords: redox potential, *β-diketonato*, manganese (III), DFT, MESP

Substituente en isomeriese effekte op die reduksie- en oksidasiepotensiaal van tris(β-diketonato)mangaan(III) komplekse: DFT en MESP analises: Die reduksie van tris(β-diketonato)mangaan(III) ([Mn(β-diketonato)$_3$]) verbindings na tris(β-diketonato) mangaan(II), asook die oksidasie daarvan tot tris(β-diketonato)mangaan(IV), is ondersoek met behulp van DFT-metodes. Die akkuraatheid van die voorspelling van die reduksiepotensiaal of oksidasiepotensiaal is baie belangrik vir die bepaling van die potensiaalomvang wat geskik is vir die ontwerp van spesifiek vereiste toepassings. Die DFT-funksionele metode M06 het die eksperimentele reduksiepotensiaal tot 'n hoër vlak van akkuraatheid weergegee, in vergelyking met die M062X en B3LYP metodes. Hierdie studie het ook getoon dat reduksie van verbindings 'n afname in entropie en ook Gibbs vrye energie, in sowel die gasfase as die oplosmiddelfase, veroorsaak het en gevolglik die hoogste waarde vir totale Gibbs reaksie-energie (ΔG_{rksie}) vir die gereduseerde verbinding getoon het, veral vir dié molekules met sterker elektron-onttrekkende groepe, soos CF_3. Dit het gelei tot 'n reduksiepotensiaalverskuiwing na meer positiewe waardes, vir dié verbindings wat CF_3 bevat. Hierdie meer positiewe reduksiepotensiaal van verbindings in die teenwoordigheid van sterker elektrononttrekkende groepe het ook 'n skuif na meer positiewe oksidasiepotensiaal tot gevolg gehad. Gevolglik kon die oksidasiepotensiaal gaandeweg nie meer binne die eksperimentele venster vir oplosmiddels waargeneem word nie. Die waardes van die molekulêre elektrostatiese oppervlakpotensiaal (MESP) minima en die MESP atoompotensiaal van die Mn atoom en sy gekoördineerde suurstofatome, dien as goeie beskrywers vir die waargeneemde eksperimentele reduksiepotensiaal en kan ook bydra om die eksperimentele reduksie van toekomstige molekules tot 'n hoë vlak van akkuraatheid te kan voorspel.

Sleutelwoorde: Redokspotensiaal, β-diketonato, mangaan (III), DFT, MESP

Introduction

Metal acetylacetonato complexes are widely used as catalysts, co-catalysts, redox mediators in dye-sensitized solar cells (DSSCs) or as electrolytes of a single-metal redox flow battery (RFB). The most well-known member of the [Mn(β-diketonato)$_3$] series of complexes, namely tris(acetylacetonato)manganese(III), is a good candidate for these applications, since it can relatively easily be reduced / oxidised to the corresponding Mn(II) and Mn(IV) analogues (Gritzner *et al.*, 1979).

For example, [Mn(β-diketonato)$_3$] showed promising results as an efficient constituent in the electrolyte of a single-metal redox flow battery (RFB) that can *inter alia* be used for the storage of the large amounts of energy produced by wind turbines and solar cells (Sleightholme *et al.*, 2011). Under standard conditions, the voltage limit for aqueous electrolytes is 1.23 V. Since the energy and power densities of an RFB are determined by the cell potential, knowledge of the redox properties and stability of the electrolyte/solvent system (containing [Mn(β-diketonato)$_3$] in this case) is important.

Evaluation of the [Mn(β-diketonato)$_3$] complex as redox mediator in dye-sensitized solar cells (DSSCs) (Carli *et al.*, 2016; Perera *et al.*, 2014), showed that the Mn^{III}/Mn^{II} couple was involved in the dye regeneration process. Although [Mn(β-diketonato)$_3$] showed a lower performance than commercially available sensitizers, it was proposed that substitution of the CH_3 groups by electron withdrawing groups (e.g. CF_3) on the acetylacetonato ligand, would pave the way to develop manganese redox couples with more positive redox potentials, which may lead to DSSCs with higher open circuit voltages.

Furthermore, tris(acetylacetonato)manganese(III) has various applications as homogeneous catalyst (Bryant *et al.*, 2002; Dewar and Nakaya, 1968; Khusnutdinov *et al.*, 2002; Magnus *et al.*, 2000; Wang and Chiba, 2009), as catalyst in the paint drying process (Bouwman and van Gorkum, 2007; Van Gorkum *et al.*, 2004) by functioning both as a radical initiator and a hydroperoxide decomposition catalyst, has a very high activity in the autoxidation of ethyl linoleate (EL, as heterogeneous catalyst (Sodhi and Paul, 2011) or as a precursor of heterogeneous catalysts (Kenvin *et al.*, 1991). As catalyst for the polymerization of benzoxazine, it was found that substitution of the CH_3 groups on the acetylacetonate ligand, by the electron withdrawing group CF_3, led to enhanced catalytic activity (Sudo *et al.*, 2010).

It was shown that the activity of Mn(III) towards oxidation and reduction in [Mn(β-diketonato)$_3$] complexes, can be tuned by substituting the CH_3 groups in the acetylacetonate ligand with groups containing different electron donating or withdrawing properties. More electron withdrawing substituents (e.g. CF_3) lead to a higher (more positive) redox potential for both the Mn^{III}/Mn^{II} and Mn^{III}/Mn^{IV} redox couples of [Mn(β-diketonato)$_3$] complexes (Freitag and Conradie, 2015). However, it is not possible to experimentally measure the redox potential of the Mn^{III}/Mn^{IV} redox couple of complexes containing electron withdrawing substituents by cyclic voltammetry, due to the limitation of the solvent window of the experimental electrochemical solvent/electrolyte system. Finding a theoretical way to calculate reliable redox potentials of the Mn^{III}/Mn^{II} and Mn^{III}/Mn^{IV} redox couples of [Mn(β-diketonato)$_3$] complexes, is therefore of importance.

We hereby thus present a computational chemistry study to theoretically calculate redox potentials of [Mn(β-diketonato)$_3$] complexes, which are in good agreement with available experimental results (Carli *et al.*, 2016; Freitag and Conradie, 2015), see Figure 1. In addition, we show that the redox potential of tris(β-*diketonato*) manganese(III) complexes can be predicted from the molecular electrostatic surface potential (MESP) of the molecules. MESP analysis is known as an important method that helps to understand several chemical phenomena, ranging from intermolecular interactions (Remya and Suresh, 2018, 2016) to various other chemical properties (Mohan *et al.*, 2013; Politzer *et al.*, 2001; Politzer and Murray, 2002) such as chemical bonding, resonance, chemical reactivity, inductive effect and prediction of the redox potential of compounds (Anjali *et al.*, 2016).

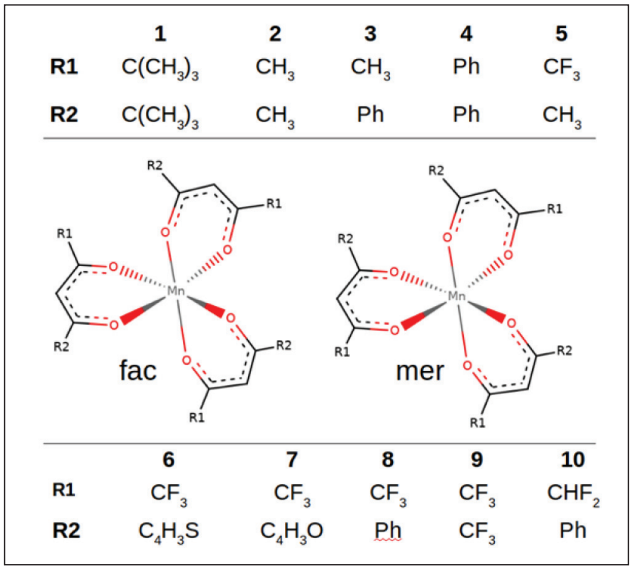

FIGURE 1: *Fac* and *mer* geometries of the [Mn(*β*-diketonato)$_3$] complexes utilized in this study. Complexes 1, 2, 4 and 9 are symmetrical, while 3, 5, 6, 7, 8 and 10 are unsymmetrically substituted.

Calculations and computational methods

Calculation of redox potential

The reduction potentials were computed using two similar free energy cycles, as described in our previous studies (Adeniyi and Conradie, 2019, 2018) and are shown in Figure 2.

In the first free energy cycle, the reduction potential (E_{cell}) is calculated as reported in the literature (Marenich *et al.*, 2014) using equation 1:

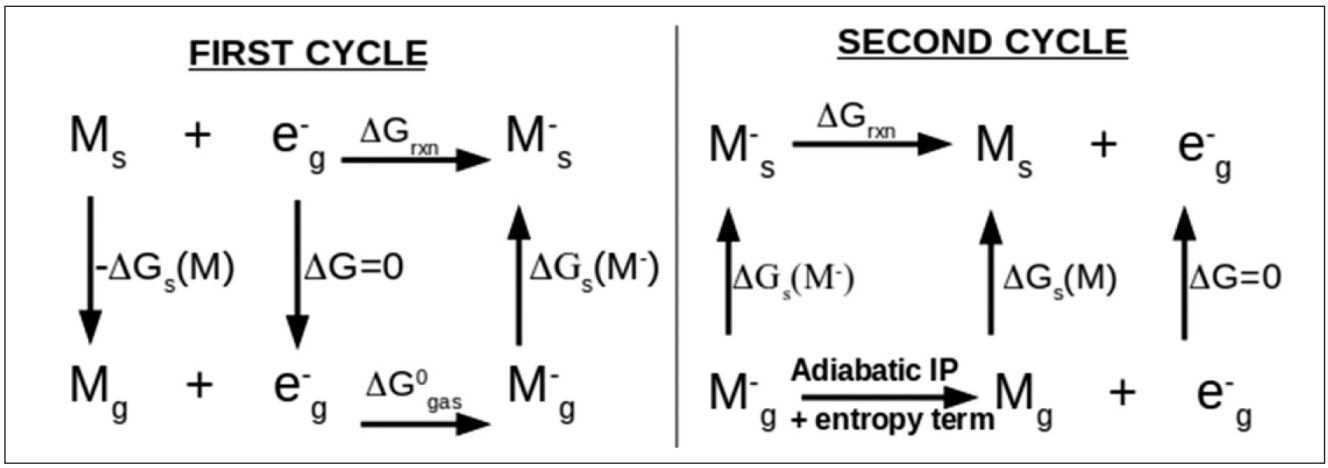

FIGURE 2: A representative scheme of the two free energy cycles that were used for the computation of the reduction potential values of the complexes (g = gas, s = solvent).

$$E_{cell}(vs\ \text{SHE}\ in\ V) = \frac{-\Delta G_{rxn}}{nF} - E_{SHE} \quad \ldots 1$$

where $\Delta G_{rxn} = \Delta G_{gas} - \Delta\Delta G_{sol}$

and $\Delta\Delta G_{sol} = \Delta G_s(M^-) - \Delta G_s(M)$

The terms $G_s(M)$ and $G_s(M^-)$ represent the free energy of solvation of the neutral and reduced states of the molecules, respectively.

In the second cycle, the reduction potential values are computed using the gas-phase calculated adiabatic ionization energies (IP) and solvation energies (ΔG_s), as reported in the literature (Fu *et al.*, 2005), using equation 2:

$$E^0(vs\ NHE\ in\ V) = IP + \frac{1}{23.06}\{-T\Delta S + \Delta G_s(M) - \Delta G_s(M^-)\} - E_{NHE} \ldots 2$$

Since the reported experimental reduction potentials of [Mn(β-diketonato)$_3$] complexes were determined *versus* the redox potential of the ferrocene couple Fc/Fc^+ (Carli *et al.*, 2016; Freitag and Conradie, 2015), the potential of the reference standard hydrogen electrode (E_{SHE} = 4.28 V) (Marenich *et al.*, 2014) in equation 1, was changed to the absolute reduction potential of Fc/Fc^+ in acetonitrile solution (4.980 V) (Namazian *et al.*, 2010). Similarly, the normal hydrogen electrode (E_{NHE} = 4.44 V) in equation 2, was changed to the absolute reduction potential of Fc/Fc^+ in acetonitrile solution (4.980 V) (Namazian *et al.*, 2010).

Calculation of electron affinity and ionization potential

The ionization potential (IP) and the electron affinity (EA) of the molecules are calculated by:

IP = E(oxd) – E(neut) ...3a
EA = E(red) – E(neut) ...3b

where E(neut), E(oxd) and E(red) are the calculated energies in the gas phase for the neutral, oxidized and reduced states of the molecules respectively.

Calculation of the MESP parameters

The molecular electrostatic surface potential (MESP) value V(r) at a point r, is calculated by the standard equation,

$$V(r) = \sum_A^N \frac{Z_A}{|r-R_A|} - \frac{\rho(r')d^3r'}{|r-r'|} \quad \ldots 4$$

where Z_A is the charge on the nucleus A at position R_A, ρ(r′) is the electron density and N is the total number of nuclei. Of the critical points (CP) on the topology analysis of MESP, a (3, +3) CP corresponds to the minimum (V_{min}); (3, -3) is the maximum (V_{max}), while (3, +1) and (3, -1) designate saddle points (Gadre and Shirsat, 2001).

DFT methods

In all calculations, the multiplicity of the neutral, reduced and oxidized forms of tris(β-*diketonato*)manganese(III) complexes was set to 5, 6 and 4 respectively and the optimized geometries were obtained using the density functional theory (DFT) functional B3LYP and the basis set 6-31+G(df,p), as implemented in method G09 (Frisch *et al.*, 2009). The energy of the optimized complexes that were used in the free energy cycle calculations, was recomputed using the DFT methods M06/6-311+G(2df,2p) and M062X/6-311+G(2df,2p) and subsequently applied in the free energy calculation, with the zero point energy computed by method B3LYP/6-31+G(df,p). These functionals were chosen since the M06 and M062X methods are known to be a very good choice for thermodynamic methods (Zhao and Truhlar, 2006), while B3LYP gives good geometries. The solvation energies were computed in acetonitrile solvent phases, using the solvation model density (SMD) of the polarizable continuum model (PCM) (Marenich *et al.*, 2009) which solved the non-homogeneous Poisson equation, by applying the integral equation formalism variant (IEF-PCM) (Skyner *et al.*, 2015).

The computation of the molecular electrostatic surface potentials (MESP) was done, using the same method B3LYP/6-31+G(df,p) as in the optimization and was computed in the acetonitrile solvent phase. All of the MESP computations were done using the G09 method (Frisch *et al.*, 2009), while further analysis of the wavefunction calculations was conducted using Multiwfn (Lu and Chen, 2012a, 2012b). The molecular rendering of the MESP isosurface of the molecules was calculated using vmd (Humphrey *et al.*, 1996) and Multiwfn (Lu and Chen, 2012a, 2012b).

Data analysis

The linear regression equation $Y = b_0 + b_1X_1$ that shows the relationship between the computed properties (X_1) and the experimental reduction potential (Y), was derived using the R statistical package (R-Core-Team, 2018). The generated regression parameters that were used to determine the level of correlation, are the intercept (b_0), slope (b_1), correlation (R^2), F-statistic, t-values, P-value and the Residual Standard Error (RSE). The level of correlation can be considered to be more optimal for values of R^2 close to unity and a very high value for both the F-statistic and t-values, combined with a lower P-value (e.g. 0.05). When relating experimental values with calculated values (here plotting experimental reduction potential *versus* computed reduction potential), the best correlation of the calculated values with the experimental values will correspond to the slope b_1 nearing unity and the intercept b_0 nearing zero. Details of the data analysis of the results of this study are given in Table S2 of the Supporting Information.

Results and discussion

Among the ten derivatives of the [Mn(β-diketonato)$_3$] complexes that were examined in this study (Figure 1), the six complexes 3, 5, 6, 7, 8, and 10 can exist as both *mer* and *fac* isomers. All calculations considered both *fac* and *mer* of these six complexes with asymmetrical substituents R1 and R2, except for the *mer* isomer of complex 7 which was excluded from this study, since its reduced geometry did not optimize correctly. Among all the complexes with both *mer* and *fac* isomers, it was only complex 10 where the *fac* isomer had a relatively lower energy than the *mer* isomer, while for complexes 3, 6, 7 and 8, the *mer* isomers were more stable (lower energy) than the *fac* (Table S1). The maximum energy difference between the *mer* and *fac* isomers was only 0.05 eV, implying that both *mer* and *fac* isomers can exist experimentally.

Reduction potential of the [Mn^{III}(β-diketonato)$_3$] complexes

The accuracy of the theoretical calculation of the reduction and oxidation potential of transition metal complexes is very significant for the customized design of the metal complexes that require some specified range of values for the reduction or oxidation potential, based on different applications. The experimental reduction potential values of all ten derivatives of [Mn(β-diketonato)$_3$] complexes (Figure 1) are available in the literature (Carli *et al.*, 2016; Freitag and Conradie, 2015). The theoretical calculation of the reduction potential was obtained using method B3LYP/6-31+G(df,p) for the optimization of geometry, calculation of zero point energy and solvation energy. The gas phase free energy in the thermodynamic cycles (Figure 2) was calculated using the calculated zero point energy and the calculated energy values obtained from M06/6-311+G(2df,2p), M062X/6-311+G(2df,2p) and B3LYP/6-31+G(df,p). Both free energy cycles 1 and 2 (Figure 2) reproduced the experimentally measured reduction potentials to a high level of accuracy, with values for R2 > 0.96, see Table S2 a and b.

Among the three DFT methods (B3LYP, M06 and M062X) used for computing the reduction potential of the Mn^{III}/Mn^{II} redox couple of complexes 1 – 10, the method M06 gave a better reproduction of the experimental values compared to M062X which overestimates the values, while B3LYP underestimates them (Table 1, Figure 3a). Most of the experimental reduction potential values were reproduced to a significant level of accuracy when using the M06 functional, except for complex 1 which showed a significant deviation from the experiment (Figure 3). This deviation might be due to the fact that the experimental reduction potential of complex 1 was obtained in dichloromethane as solvent, while those of complexes 2 – 10 was obtained in acetonitrile instead. Also all computed reduction potentials were obtained using acetonitrile as solvent in the free energy cycles from Figure 2. However, when comparing experimental and theoretical redox values, experimental values obtained under the same experimental conditions are preferred. Recalculation of the reduction potential of complex 1, using the M06 functional and dichloromethane as solvent instead of acetonitrile, produced a slightly better calculated value compared to the experimentally determined one (-0.964 V), namely -0.737 and -0.830 V for the first and second thermodynamic cycles (Figure 2), respectively. The first thermodynamic cycle performed better in reproducing the experimental results when the M06 functional was used (Figure 3a), with a lowest mean absolute deviation (MAD) value of 0.102 eV (using the symmetrically substituted complexes together with the *fac* isomers of the unsymmetrical complexes). The MAD value when using the second thermodynamic cycle was 0.145 eV (Table 1). Although the calculated reduction potential values deviated slightly from the experimental ones, the correlation between these values was very high. The correlation results from the M062X (R^2 = 0.973 to 0.975) and B3LYP (R^2 = 0.961 to 0.966) methods were as high as those of M06 (R^2 = 0.970 to 0.973), even though they had a higher deviation from reproducing the experimental values compared to M06 (Table S2 a and b, Figure S1 a and b). The intercept of the linear regression equation between the experimental and the computed reduction potential using the M06 method, approached zero (0.030 and 0.035 eV respectively for the *fac* and *mer* isomers), indicating a

significant level of reproducing the experiment. However, a larger deviation was obtained for M062X (with negative values indicating overestimation of reduction potential) and B3LYP (with positive values indicating underestimation of reduction potential) (Table S2 a and b).

While the effect of the electron withdrawing tendency of substituents R1 and R2 on the β-diketonato ligands in the [Mn(β-diketonato)$_3$] complexes 1 – 10 (Figure 1) was clear from the experimental reduction potential values (which were also reproduced in the theoretical calculation), the theoretical method additionally provided better insight into the effects of isomers on the change in thermodynamic properties of the observed reduction potential values. The values of the computed change in the thermodynamic parameters are provided in Table S3.

There was only a small difference in the values of the reduction potential of the *fac* and *mer* isomers, Table 1. The results from the three methods M06, M062X and B3LYP, using either the first or the second free energy cycle, clearly (Figure 2) showed the computed reduction potential of the *mer* isomers of complexes 3 and 8 to be generally larger (more positive) than that of the *fac* isomer. The relative difference in the reduction potential of the *mer* and *fac* isomers of 5, 6 and 10 depended on the method used. Method M06 with the first thermodynamic cycle best reproduced the experimental results. However, while the computed reduction potential of the *mer* isomer of complex 5 also was larger (more positive) when compared to its *fac* isomer, the reverse was the case for complexes 6 and 10.

It was obvious from both experimental and theoretical reduction potential values that a combination of two symmetrical strong electron donating -C(CH$_3$)$_3$ substituents per β-diketonato ligand, as in complex 1, resulted in a more negative reduction value. On the other hand, two symmetrical strongly electron withdrawing CF$_3$ substituents per β-diketonato ligand, as in complex 9, resulted in a more positive reduction value (Figure 3 and Table 1). The asymmetrical combination of both an electron withdrawing group and an electron donating group, as in complexes 5 and 10, resulted in a higher and less negative reduction potential, thereby enhancing the reduction activity of those complexes. The results of the change in thermodynamic properties in going from the neutral to the reduced form, are shown in Table S3. A decrease in the entropy, as well as the Gibbs free energy, both of the gas phase and solvent phase of the system, was observed from the neutral state to reduced state, which consequently resulted in a favourable

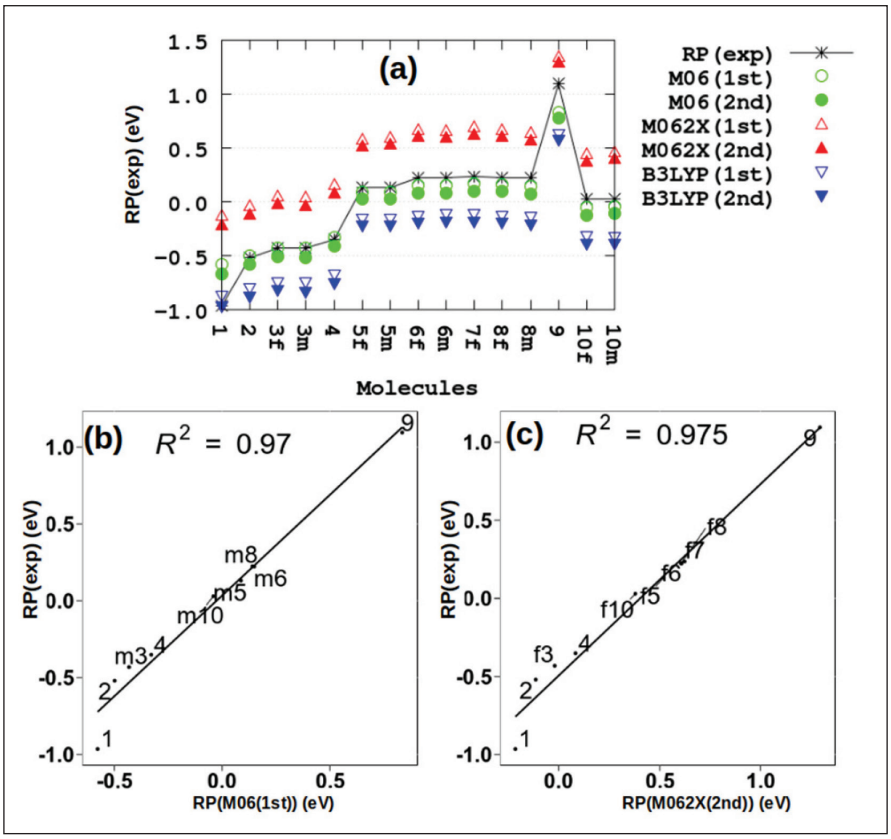

FIGURE 3: Plots of (a) The experimental reduction potential (RP(exp)) of the Mn^{III}/Mn^{II} redox couple of [Mn(*β*-diketonato)$_3$] complexes 1 – 10 and the computed reduction potential using methods M06, M062X and B3LYP; (b) The correlation of the experimental reduction potential with the computed values of the symmetrically substituted complexes 1, 2, 4 and 9, as well as the *mer* isomers of unsymmetrical complexes 3, 5, 6, 7, 8, and 10, calculated by method M06 using the first energy cycle; (c) Computed values of the symmetrically substituted complexes 1, 2, 4 and 9, and the *fac* isomers of unsymmetrical complexes 3, 5, 6, 7, 8, and 10, calculated by method M062X using the second energy cycle. All reduction potentials are in V *vs* Fc/Fc$^+$.

TABLE 1: The computed reduction potential of the Mn^{III}/Mn^{II} redox couple of complexes 1 – 10, using the M06, M062X and B3LYP functionals, following both the first and second thermodynamic cycles, compared with the experimental reduction potential (in the first column). The mean absolute deviations (MAD) were determined, by comparing the symmetrically substituted molecules with either the *mer* or *fac* isomers of the unsymmetrically substituted compounds, as indicated. All reduction potentials are in V *vs* Fc/Fc^+.

	RP(exp)	M06(1st)	M06(2nd)	M062X(1st)	M062X(2nd)	B3LYP(1st)	B3LYP(2nd)
1	-0.964	-0.578	-0.671	-0.122	-0.215	-0.877	-0.970
2	-0.520	-0.499	-0.576	-0.038	-0.114	-0.806	-0.883
3f	-0.431	-0.431	-0.505	0.053	-0.020	-0.747	-0.820
3m	-0.431	-0.432	-0.515	0.049	-0.034	-0.754	-0.837
4	-0.351	-0.329	-0.408	0.162	0.083	-0.676	-0.755
5f	0.132	0.090	0.027	0.583	0.520	-0.160	-0.223
5m	0.132	0.087	0.023	0.595	0.532	-0.164	-0.227
6f	0.223	0.148	0.085	0.671	0.608	-0.134	-0.197
6m	0.223	0.149	0.084	0.661	0.595	-0.118	-0.184
7f	0.236	0.171	0.099	0.695	0.623	-0.116	-0.187
8f	0.225	0.161	0.098	0.669	0.606	-0.134	-0.197
8m	0.225	0.140	0.069	0.645	0.574	-0.142	-0.213
9	1.095	0.835	0.780	1.349	1.294	0.627	0.572
10f	0.030	-0.051	-0.122	0.450	0.379	-0.320	-0.391
10m	0.030	-0.041	-0.108	0.465	0.398	-0.327	-0.394
MAD(*fac*)		**0.102**	**0.145**	**0.480**	**0.409**	**0.319**	**0.373**
MAD(*mer*)		**0.107**	**0.150**	**0.481**	**0.408**	**0.317**	**0.370**

total thermodynamic reaction free energy (ΔG_{rxt}) of reduction of the systems. Complex 9 which had the highest, most positive, reduction potential, was also associated with the highest value of ΔG_{rxt} but lowest change in the solvation Gibbs free energy.

Oxidation potential of the [Mn^{III}(β-diketonato)$_3$] complexes

The experimental oxidation potential of the Mn^{III}/Mn^{IV} redox couple of the complexes that are available in literature (Carli *et al.*, 2016; Freitag and Conradie, 2015) and the computed values using the M06 DFT functional method, are shown in Table 2. The available experimental oxidation potentials of the complexes were reproduced to a very high level of accuracy for both the first and second cycle (MAD = 0.089 and 0.054), using results of the symmetrically substituted molecules and the unsymmetrical *fac* isomers. Similarly as was observed in the computation of the reduction potential, the highest deviation from the experimental oxidation potential was again complex 1, which can be explained by the different experimental conditions used (see above) compared to the other molecules.

This study enabled the calculation and corresponding correlation of the available experimental oxidation potentials for complexes 1 – 4 and 10. The oxidation potential values of the other complexes (5 – 9) were not available and mostly not experimentally feasible within the experimental solvent window, but could be obtained by computation. The presence of CF_3 in complexes 5 – 9 had a much larger effect on the oxidation potential than group CHF_2 in complex 10, resulting in a correspondingly higher value of the oxidation potential for complexes 5 – 9, consequently making it less feasible to be oxidized. The higher computed oxidation potentials for complexes 5 – 9 also explain why the oxidation potential could not experimentally be measured in CH_3CN, which has an upper limit of *ca.* 1.1 V *vs* Fc/Fc^+ to be observable.

An excellent correlation was observed between the experimental reduction potential of the complex and the computed oxidation potential, either using either the first or second thermodynamic cycle (Figure 4). The oxidation potential was directly proportional to the observed reduction potential. This relationship was expected, since the difference in potential between two successive redox processes of a series of similar molecules are generally within a narrow range. For example, for Ru(III) complexes, the average potential difference between the two successive redox processes' two Ru^{III}/Ru^{II} and Ru^{III}/Ru^{IV} redox couples was 1.2 V to 1.7 V (Bag *et al.*, 1988; Chattopadhyay *et al.*, 1990; Cornioley-Deuschel and Von Zelewsky, 1987; Eskelinen *et al.*, 2005; Holligan *et al.*, 1992; Lahiri *et al.*, 1987; Rillema and Jones, 1979; Yang *et al.*, 1993). In this study, the experimentally observed potential difference between the Mn^{III}/Mn^{II} and Mn^{III}/Mn^{IV} redox couples of [Mn(β-diketonato)$_3$] complexes, was 0.9 – 1.2 V. Consequently, complex 1 with the most negative reduction potential (-0.964 V *vs* Fc/Fc^+ experimentally) had the lowest oxidation potential value (0.291 V *vs* Fc/Fc^+ experimentally), while complex 9 with the most positive reduction potential (1.095 V *vs* Fc/Fc^+ experimentally), exhibited the highest oxidation potential (2.1 V *vs* Fc/Fc^+ M06 calculated).

Electron affinity and ionization potential of the [Mn^{III}(β-diketonato)$_3$] complexes

The values of the electron affinities (EA) were computed for the complexes during their reduction reaction, using M06, M062X and B3LYP (Table 3) methodologies, while their corresponding ionization potentials (IP) during the oxidation reaction were computed using M06. As expected, the complexes with CF_3 substituents had the highest values of the electron affinity, especially complex 9 with two CF_3 substituents on each β-diketonato ligand. The effect of group CHF_2 on the electron affinity was less compared to the effect of CF_3, implying that the complexes with the electron withdrawing CF_3 groups have the highest affinity

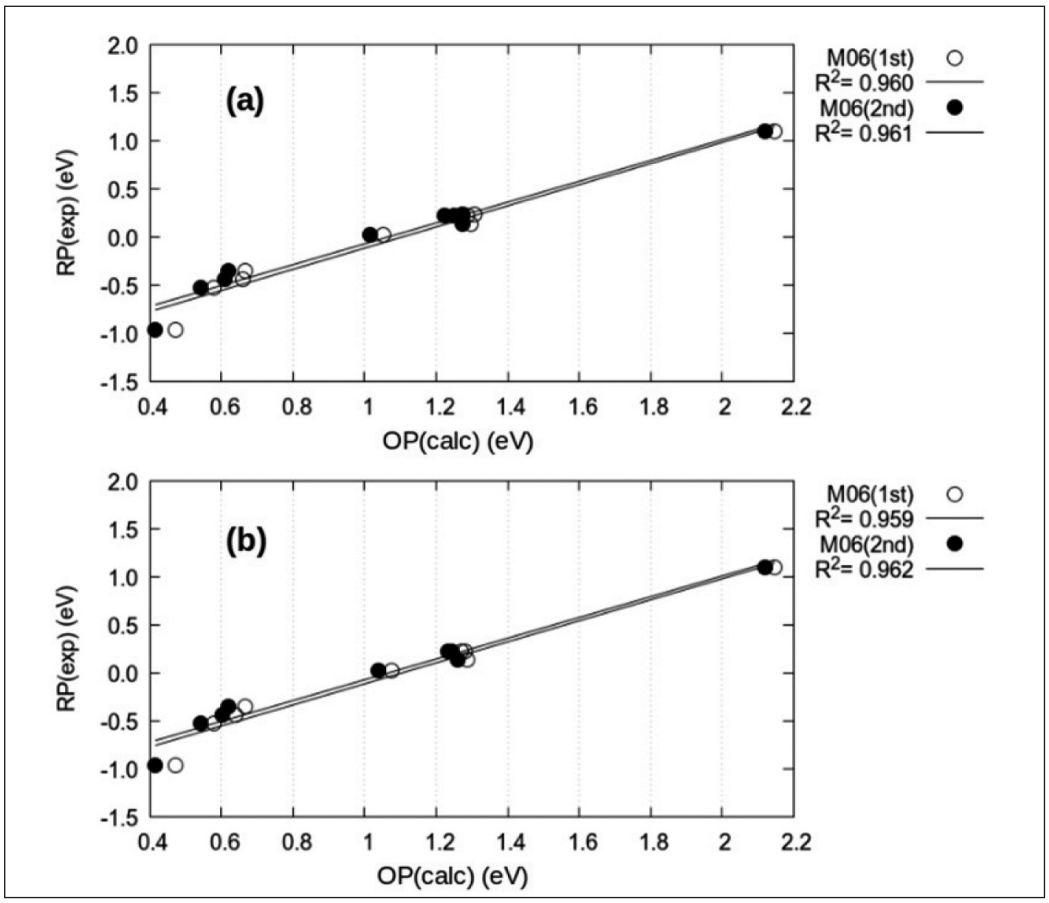

FIGURE 4: Correlation of the experimental reduction potential, RP(exp), of the Mn^{III}/Mn^{II} redox couple with the computed oxidation potential, OP(calc), of the Mn^{III}/Mn^{IV} redox couple of complexes 1 – 10, using the symmetrically substituted complexes with (a) firstly the *fac* isomers and (b) then the *mer* isomers of the unsymmetrically substituted complexes. All oxidation and reduction potentials are in V *vs* Fc/Fc^{+}.

TABLE 2: The oxidation potential (OP) values of the Mn^{III}/Mn^{IV} redox couple of the ten complexes, using the M06 functional method for both the first and second thermodynamic cycles. All oxidation potentials are in V *vs* Fc/Fc^{+}.

	OP(exp)	OP(M06(1st))	OP(M06(2nd))
1	0.291	0.472	0.414
2	0.571	0.579	0.542
3f	0.593	0.658	0.607
3m		0.639	0.601
4	0.614	0.665	0.617
5f		1.298	1.273
5m		1.287	1.260
6f		1.286	1.250
6m		1.269	1.235
7f		1.306	1.275
7m		1.290	1.249
8f		1.269	1.223
8m		1.281	1.243
9		2.147	2.120
10f	0.914[a]	1.053	1.014
10m		1.075	1.039
MAD		**0.089**	**0.054**

[a] Experimental OP was not assigned to 10f or 10m.

for electrons. The same pattern was observed for the ionization potentials, where complex 9 with two CF_3 substituents on each β-diketonato ligand had the highest value of the oxidation potential, implying that complex 9 will be the most difficult to oxidize of complexes 1 – 10.

There was a high level of correlation between the experimental reduction potential (cell potential in V, required to add an electron to the molecule) and the calculated electron affinity (amount of energy in eV released when an electron is added to a molecule in the gaseous state) of the complexes, as indicated by the R^2 values which were in a very close range of 0.927 to 0.935 (Figure S1 (c) and (d), Table S2 (c) and (d)), depending on the methods and selected isomers. The electron affinity was directly proportional to the experimentally observed reduction potential. The computed electron affinities also had a reasonable level of correlation with the computed ionization potential (R^2 = 0.876 to 0.893, depending on the methods, Figure S2). This observation was consistent with the correlation between the experimental reduction potential of the molecule and the computed oxidation potential (Figure 4), as obtained and motivated in Section 3.2.

TABLE 3: The ionization potential (IP) and electron affinity (EA) of the complexes in eV.

	EA(M06)	EA(M062X)	EA(B3LYP)	IP(M06)
1	-2.658	-3.114	-2.359	6.495
2	-2.519	-2.980	-2.211	6.724
3f	-2.726	-3.210	-2.410	6.551
3m	-2.720	-3.201	-2.398	6.578
4	-2.900	-3.391	-2.553	6.464
5f	-3.516	-4.009	-3.266	7.755
5m	-3.500	-4.009	-3.250	7.775
6f	-3.570	-4.093	-3.288	7.298
6m	-3.538	-4.050	-3.270	7.319
7f	-3.540	-4.064	-3.254	7.332
8f	-3.613	-4.121	-3.318	7.358
8m	-3.580	-4.085	-3.298	7.389
9	-4.561	-5.075	-4.353	8.834
10f	-3.364	-3.865	-3.095	7.182
10m	-3.398	-3.904	-3.113	7.155

Molecular electrostatic potential (MESP) of the [Mn^{III}(β-diketonato)$_3$] complexes

The application of the MESP analysis ranges from being used as descriptor for reactivity to determining the stability of both chemical and biological systems (Anjali and Suresh, 2018; Remya and Suresh, 2018). Typical MESP parameters, such as the atomic potential (V_{atom}) and minimum potential (V_{min}), have successfully been used to determine the total electronic effect of ligands (eeL) and to predict the reduction potential of molecules (Anjali *et al.*, 2016; Anjali and Suresh, 2018).

The computed values of the MESP minima (V_{min}), the electrostatic potential of the Mn centre (V_{Mn}), the lowest value (indicated by l) and the highest value (indicated by h) of the electrostatic potential of the coordinating O atoms, are shown in Table 4 both for the neutral and reduced states of the molecules. In all the computed MESP parameters, the values of V_{Mn} were higher than for V_O and V_{min}. Complex 9 with two CF_3 groups per β-diketonato ligand, had the highest values of the computed MESP parameters, followed by complexes 5 to 8 with one CF_3 group each per β-diketonato ligand. The results showed, similarly as was found for the calculated EA, IP, reduction and oxidation potentials, that the CF_3 group has a stronger effect on the MESP parameters of the complexes, than the CHF_2 group in complex 10. The presence of a strong electron withdrawing CF_3 group resulted in a less negative (smaller absolute value) MESP parameter. The MESP parameters of the *mer* isomers were less negative than their corresponding *fac* isomers (Table 4). It was also obvious that the MESP parameters were more negative (larger absolute value) for the neutral states relative to their reduced states. The representative features of the V_{min} and V_{Mn} values for complexes 2, 9 and 10 (both *fac* and *mer*) are shown in Figure 5. It is clear that the V_{min} of each molecule was located between two oxygen atoms of two different coordinating ligands and was preferentially found either on a side with a mixture of strong electron withdrawing and electron donating groups, as in 10 *mer* (on the side with CF_3 and Ph substituent), or on a side with a combination of two electron withdrawing group, as in 10 *fac* (on the side with two CF_3 substituents) (see Figure 5).

The regression equations provided below and further summarized in Table S2 of the Supporting Information, are expressed in terms of the relative values of V_{min}, V_{Mn} and V_O, namely ΔV_{min}, ΔV_{Mn} and ΔV_O, which were calculated by subtracting the corresponding values of complex 2 (with only CH_3-substitutents per β-diketonato ligand as reference complex), from each of the other specified complexes. Among all the regression fits, the best results based on the regression parameters (Table S2 (e) – (j)) were obtained, by using the symmetrically substituted complexes and the *mer* isomers of the unsymmetrically substituted complexes

TABLE 4: Computed electrostatic potential of the two O atoms (the O with lowest value indicated by l and highest value indicated by h), using the *mer* isomers of both the neutral complex and reduced complex (*) where applicable. The V_{Mn} and V_O values are in au, while V_{min} values are in kcal/mol. The calculation of MAD excludes complex 1, which seriously deviated from the observed trends. Predicted reduction potential (RP) values (V *vs* Fc/Fc^+) were obtained by application of the indicated regression fits.

		MESP parameter								RP(pred) from regression fit (using *mer* + symmetrical)		
	RP(exp)	V_{min}	V_{*min}	V_{Mn}	V_{*Mn}	V_{lO}	V_{hO}	V_{*lO}	V_{*hO}	ΔV_{*min}	ΔV_{*Mn}	ΔV_{*lO}
1	-0.964	-45.92	-128.36	-109.33	-109.59	-22.35	-22.32	-22.49	-22.49	-0.221	-0.357	-0.428
2	-0.520	-51.00	-135.53	-109.33	-109.61	-22.35	-22.32	-22.50	-22.50	-0.479	-0.602	-0.494
3f	-0.431	-54.19	-134.77	-109.33	-109.60	-22.36	-22.32	-22.50	-22.49	-0.451	-0.471	-0.454
3m	-0.431	-53.12	-134.31	-109.33	-109.60	-22.36	-22.32	-22.50	-22.49	-0.435	-0.448	-0.462
4	-0.351	-52.87	-132.31	-109.33	-109.59	-22.36	-22.33	-22.49	-22.49	-0.363	-0.351	-0.390
5f	0.132	-41.63	-120.93	-109.28	-109.56	-22.31	-22.27	-22.45	-22.45	0.047	0.188	0.213
5m	0.132	-37.06	-118.56	-109.28	-109.56	-22.31	-22.27	-22.45	-22.45	0.132	0.184	0.219
6f	0.223	-49.75	-122.91	-109.29	-109.55	-22.33	-22.29	-22.46	-22.45	-0.024	0.211	0.140
6m	0.223	-45.94	-121.57	-109.30	-109.55	-22.32	-22.29	-22.46	-22.45	0.024	0.207	0.142
7f	0.236	-49.64	-122.98	-109.29	-109.55	-22.33	-22.28	-22.46	-22.45	-0.027	0.210	0.157
7m	0.236	-43.12		-109.29		-22.32	-22.29					
8f	0.225	-46.58	-121.04	-109.29	-109.55	-22.32	-22.28	-22.45	-22.45	0.043	0.272	0.200
8m	0.225	-39.12	-118.02	-109.29	-109.55	-22.31	-22.28	-22.45	-22.45	0.152	0.260	0.218
9	1.095	-15.14	-94.12	-109.22	-109.50	-22.25	-22.22	-22.40	-22.40	1.012	1.006	1.068
10f	0.030	-32.03	-110.22	-109.29	-109.56	-22.32	-22.29	-22.46	-22.45	0.432	0.155	0.118
10m	0.030	-30.03	-112.91	-109.29	-109.56	-22.32	-22.29	-22.46	-22.45	0.335	0.148	0.100
MAD										0.137	0.051	0.053

where applicable, with the MESP parameters from the reduced state of the complexes (values of the reduced state are indicated by *). Predicting the experimental reduction potential from the best fits, from $\Delta V_{*min}(mer)$, $\Delta V_{*Mn}(mer)$ and $\Delta V_{*lO}(mer)$, yields the regression equations:

$$RP(pred)(\Delta V_{*min}) = -0.479+0.036*(\Delta V_{*min}) \quad R^2 = 0.922 \quad \ldots 5a$$
$$RP(pred)(\Delta V_{*Mn}) = -0.602+14.99*(\Delta V_{*Mn}) \quad R^2 = 0.983 \quad \ldots 5b$$
$$RP(pred)(\Delta V_{*lO}) = -0.494+15.781*(\Delta V_{*lO}) \quad R^2 = 0.988 \quad \ldots 5c$$

The plots for the correlation of the computed MESP parameters with the experimental reduction potentials are

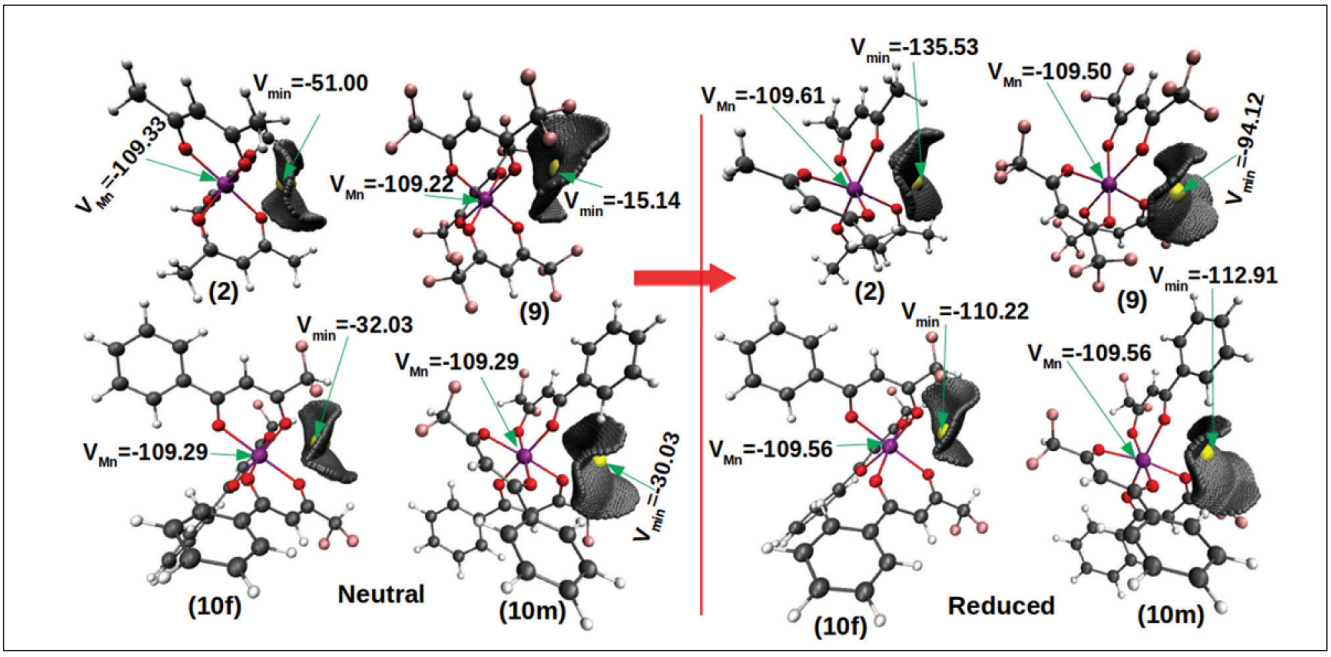

FIGURE 5: The MESP isosurface, showing the minimum electrostatic point (V_{min} in kcal/mol) and atomic potential of Mn (V_{Mn} in au) for complexes 2 (two CH_3 groups per β-diketonato ligand), 9 (two CF_3 groups per β-diketonato ligand), 10 *fac* and 10 *mer* (one CH_3 and one CF_3 group per β-diketonato ligand), in both their neutral and reduced states, respectively. 1 a.u. = 627.51 kcal/mol.

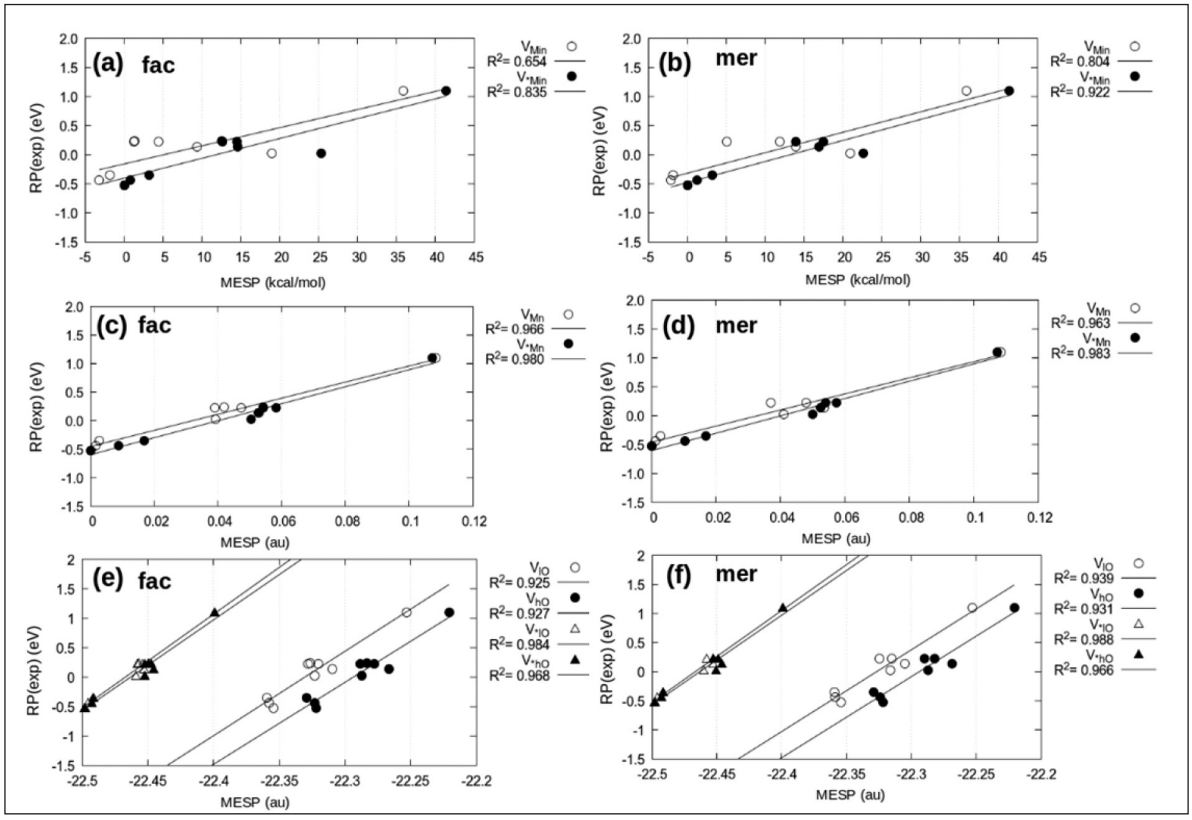

FIGURE 6: Correlation of the experimental reduction potential with (a) and (b) the minimum electrostatic point (V_{min} in kcal/mol), (c) and (d) the atomic potential of Mn (V_{Mn} in au), and (e) and (f) the atomic potential of the two O atoms (V_O in au, the O with lowest value indicated by l and O with highest value indicated by h), for both the *fac* (a, c and e) and *mer* (b, d and f) isomers of the neutral complex as well as the reduced complex (*), where applicable. All reduction potentials are in V *vs* Fc/Fc^+. 1 a.u. = 627.51 kcal/mol.

shown in Figure 6, which indicate a significant correlation. The values of the predicted reduction potential, using the three equations (5a – 5c) above, are shown in Table 4. It is obvious from the MAD values that the predictions from ΔV_{*Mn} (0.051) and ΔV_{*lO} (0.053) best reproduced the experimental values when compared to ΔV_{*min} (0.137). The highest deviation from the experimental values was observed in complex 1, just as was observed for all the relationships relating the experimental reduction potential of complex 1 with various computed values obtained from the various DFT methods. Apart from complex 1, the experimental reduction potential values of the other complexes were reproduced to reasonable accuracy, using the regression formulae obtained from both ΔV_{*Mn} and ΔV_{*lO}.

Conclusion

A reliable theoretical method for calculating the redox potential of the Mn^{III}/Mn^{II} and Mn^{III}/Mn^{IV} redox couples for tris(β-*diketonato*)manganese(III) complexes, has been presented. This method enables the prediction of the redox potentials of unknown [Mn(β-diketonato)$_3$] complexes, and thereby also their activity for a specific application, prior to the chemical synthesis. In addition, the redox potential of Mn^{III}/Mn^{IV} redox couples of [Mn(β-diketonato)$_3$] complexes that cannot be measured experimentally, can be determined theoretically using this methodology.

Many of the experimental reduction potentials were reproduced to a significant level of accuracy, except complex 1 which deviated significantly from the experimental value, probably since the latter was not obtained under the same experimental conditions as complexes 2 – 10: it was obtained in dichloromethane for complex 1, while the experimental reduction potentials of complexes 2 – 10, as well as the computed reduction potentials of all ten complexes, were obtained in acetonitrile instead. Among the three DFT methods, the method M06 (MAD=0.102 eV) reproduced the experimental reduction potentials better than both M062X (MAD=0.408) which overestimated the values and B3LYP (MAD=0.317) which underestimated the values. The three DFT methods reproduced the experimental trend to a high level of significance. R^2 values of 0.970, 0.973 and 0.961 were obtained for M06, M062X and B3LYP respectively, using the first thermodynamic cycle (Figure 2) which gives the lowest deviation from experimental values. The *mer* isomers were found to have relatively higher stability in terms of the energy than the *fac* isomers in complexes 3, 5, 6, 7 and 8, while instead the *fac* isomer was more stable for complex 10. This trend was also reflected in the computed reduction potentials, where the value for the *fac* isomer of complex 10 was larger than that of the *mer* isomer, which was the reverse in complexes 3 and 8. Increased strength of the electron donating group on the β-diketonato ligands, resulted in a more negative reduction potential for those [Mn(β-diketonato)$_3$] complexes, while increased strength of the electron withdrawing group, yielded a more positive reduction potential instead. Asymmetrical combination of both an electron withdrawing and an electron donating group, resulted in a lower reduction potential, thereby enhancing the reduction of the system. The reduction of the complexes resulted in a decrease in the entropy and the Gibbs free energy of both the gas phase and solvent phase, consequently giving the highest value of total Gibbs free energy for the reaction (ΔG_{rxt}.). This thermodynamic effect was more prominent in a system with strong electron withdrawing groups, such as complex 9 with two CF_3 groups per β-diketonato ligand.

The computational study also reproduced the available experimental oxidation potentials of symmetrical complexes 2, 3, 4 and 10, but indicated a significant deviation for complex 1, as was also observed for its reduction potential. The results provided insight into the oxidation potentials of complexes 5, 6, 7, 8 and 9 that were not experimentally measurable, since they fall outside the experimental solvent window. There was a significant correlation, showing that the complexes with higher reduction potential, like complex 9, also have a higher oxidation potential, with higher ionization potential and corresponding higher electron affinity.

The MESP minima were preferentially found in the region between two coordinating oxygen atoms of different β-diketonato ligands. For *mer* isomers, the MESP minima were preferentially located near the region of the electron withdrawing substituent. The MESP parameter of the reduced state of the complexes best correlated and predicted the experimental reduction potential values. The MESP value of the Mn atom or any of the coordinating oxygen atoms that had the lowest value of electrostatic potential, gave the most accurate prediction of the experimental reduction potential.

Author contributions

JC and AA conceptualized the project; AA did the computational work and wrote the draft publication with editing done by JC.

Acknowledgment

The authors would like to acknowledge the University of the Free State and National Research Foundation in South Africa for financial support (Grant Nos: 109673, 113327 and 96111). The CHPC of South Africa, the Norwegian Supercomputing Program (UNINETT Sigma2, Grant No. NN9684K) and the High Performance Computing facility of the UFS are all acknowledged for computer time.

Supporting Information

Additional graphs and tables are provided in the Supporting Information.

References

Adeniyi, A.A., Conradie, J., 2019. Computational insight into the contribution of para-substituents on the reduction potential, proton affinity, and electronic properties of nitrobenzene compounds. J. Mol. Model. 25, 78. https://doi.org/10.1007/s00894-019-3946-2

Adeniyi, A.A., Conradie, J., 2018. Influence of substituents on the reduction potential and pKa values of β-diketones tautomers: A theoretical study. Electrochim. Acta. https://doi.org/https://doi.org/10.1016/j.electacta.2018.12.030

Anjali, B.A., Sayyed, F.B., Suresh, C.H., 2016. Correlation and Prediction of Redox Potentials of Hydrogen Evolution Mononuclear Cobalt Catalysts via Molecular Electrostatic Potential: A DFT Study. J. Phys. Chem. A 120, 1112−1119. https://doi.org/10.1021/acs.jpca.5b11543

Anjali, B.A., Suresh, C.H., 2018. Electronic effect of ligands vs. reduction potentials of Fischer carbene complexes of chromium : a molecular electrostatic potential analysis. New J. Chem. 42, 18217–18224. https://doi.org/10.1039/C8NJ04184A

Bag, N., Lahiri, G.K., Bhattacharya, S., Falvello, L.R., Chakravorty, A., 1988. Ruthenium phenolates. Chemistry of a family of RuIIIO6 tris chelates. Inorg. Chem. 27, 4396–4402. https://doi.org/10.1021/ic00297a014

Bouwman, E., van Gorkum, R., 2007. A study of new manganese complexes as potential driers for alkyd paints. J. Coatings Technol. Res. 4, 491–503. https://doi.org/10.1007/s11998-007-9041-0

Bryant, J.R., Taves, J.E., Mayer, J.M., 2002. Oxidations of Hydrocarbons by Manganese(III) Tris(hexafluoroacetylacetonate). Inorg. Chem. 41, 2769–2776. https://doi.org/10.1021/ic025541z

Carli, S., Benazzi, E., Casarin, L., Bernardi, T., Bertolasi, V., Argazzi, R., Caramori, S., Bignozzi, C.A., 2016. On the stability of manganese tris(β-diketonate) complexes as redox mediators in DSSCs. Phys. Chem. Chem. Phys. 18, 5949–5956. https://doi.org/10.1039/c5cp05524e

Chattopadhyay, S., Bag, N., Basu, P., Lahiri, G.K., Chakravorty, A., 1990. Oxo transfer and metal oxidation in the reaction of [Ru(PPh3)3Cl2] with m-chloroperbenzoic acid: structure of [Ru(PPh3)2(m-ClC6H4CO2)Cl2]. J. Chem. Soc. Dalt. Trans. 3389–3392. https://doi.org/10.1039/DT9900003389

Cornioley-Deuschel, C., Von Zelewsky, A., 1987. Complexes of platinum(II) and palladium(II) with the 2,2′-biphenyldiyl dianion as a .sigma.-bonded chelate ligand. Inorg. Chem. 26, 3354–3358. https://doi.org/10.1021/ic00267a028

Dewar, M.J.S., Nakaya, T., 1968. Oxidative coupling of phenols. J. Am. Chem. Soc. 90, 7134–7135. https://doi.org/10.1021/ja01027a051

Eskelinen, E., Da Costa, P., Haukka, M., 2005. The synthesis and electrochemical behavior of ruthenium(III) bipyridine complexes: [Ru(dcbpy)Cl4]− (dcbpy=4,4′-dicarboxylic acid-2,2′-bipyridine) and [Ru(bpy)Cl3L] (L=CH3OH, PPh3, 4,4′-bpy, CH3CN). J. Electroanal. Chem. 579, 257–265. https://doi.org/https://doi.org/10.1016/j.jelechem.2005.02.014

Freitag, R., Conradie, J., 2015. Electrochemical and Computational Chemistry Study of Mn(β-diketonato)3 complexes. Electrochim. Acta 158, 418–426. https://doi.org/https://doi.org/10.1016/j.electacta.2015.01.147

Frisch, M.J., Trucks, G.W., Schlegel, H.B., Scuseria, G.E., Robb, M.A., Cheeseman, J.R., Scalmani, G., Barone, V., Mennucci, B., Petersson, G.A., Nakatsuji, H., Caricato, M., Li, X., Hratchian, H.P., Izmaylov, A.F., Bloino, J., Zheng, G., Sonnenberg, J.L., Hada, M., Ehara, M., Toyota, K., Fukuda, R., Hasegawa, J., Ishida, M., Nakajima, T., Honda, Y., Kitao, O., Nakai, H., Vreven, T., Montgomery Jr., J.A., Peralta, J.E., Ogliaro, F., Bearpark, M.J., Heyd, J., Brothers, E.N., Kudin, K.N., Staroverov, V.N., Kobayashi, R., Normand, J., Raghavachari, K., Rendell, A.P., Burant, J.C., Iyengar, S.S., Tomasi, J., Cossi, M., Rega, N., Millam, N.J., Klene, M., Knox, J.E., Cross, J.B., Bakken, V., Adamo, C., Jaramillo, J., Gomperts, R., Stratmann, R.E., Yazyev, O., Austin, A.J., Cammi, R., Pomelli, C., Ochterski, J.W., Martin, R.L., Morokuma, K., Zakrzewski, V.G., Voth, G.A., Salvador, P., Dannenberg, J.J., Dapprich, S., Daniels, A.D., Farkas, Ö., Foresman, J.B., Ortiz, J. V, Cioslowski, J., Fox, D.J., 2009. Gaussian 09.

Fu, Y., Liu, L., Yu, H., Wang, Y., Guo, Q., 2005. Quantum-Chemical Predictions of Absolute Standard Redox Potentials of Diverse Organic Molecules and Free Radicals in Acetonitrile. J. Am. Chem. Soc. 127, 7227–7234. https://doi.org/10.1021/ja0421856

Gadre, S.R., Shirsat, R.N., 2001. Electrostatics of Atoms and Molecules. Universities Press, India.

Gritzner, G., Murauer, H., Gutmann, V., 1979. Solvent and Salt Effects on the Redox Behaviour of trisacetylacetonatomanganese(III). J. Electroanal. Chem. 101, 185–200.

Holligan, B.M., Jeffery, J.C., Norgett, M.K., Schatz, E., Ward, M.D., 1992. The co-ordination chemistry of mixed pyridine–phenol ligands; spectroscopic and redox properties of mononuclear ruthenium complexes with (pyridine)6–(phenolate) donor sets (x= 1 or 2). J. Chem. Soc. Dalt. Trans. 3345–3351. https://doi.org/10.1039/DT9920003345

Humphrey, W., Dalke, A., Schulten, K., 1996. VMD: visual molecular dynamics. J. Mol. Graph. 14, 27-28,33-38.

Kenvin, J.C., White, M.G., Mitchell, M.B., 1991. Preparation and characterization of supported mononuclear metal complexes as model catalysts. Langmuir 7, 1198–1205. https://doi.org/10.1021/la00054a030

Khusnutdinov, R.I., Shchadneva, N.A., Baiguzina, A.R., Lavrentieva, Y.Y., Dzhemilev, U.M., 2002. Generation of alkyl hypochlorites in oxidation of alcohols with carbon tetrachloride catalyzed by vanadium and manganese compounds. Russ. Chem. Bull. 51, 2074–2079. https://doi.org/10.1023/A:1021668011691

Lahiri, G.K., Bhattacharya, S., Ghosh, B.K., Chakravorty, A., 1987. Ruthenium and osmium complexes of N,O chelators: syntheses, oxidation levels, and distortion parameters. Inorg. Chem. 26, 4324–4331. https://doi.org/10.1021/ic00273a010

Lu, T., Chen, F., 2012a. Multiwfn: a multifunctional wavefunction analyzer. J. Comput. Chem. 33, 580–592. https://doi.org/10.1002/jcc.22885

Lu, T., Chen, F., 2012b. Quantitative analysis of molecular surface based on improved Marching Tetrahedra algorithm. J. Mol. Graph. Model. 38, 314–323. https://doi.org/https://doi.org/10.1016/j.jmgm.2012.07.004

Magnus, P., Payne, A.H., Waring, M.J., Scott, D.A., Lynch, V., 2000. Conversion of α,β-unsaturated ketones into α-hydroxy ketones using an Mn(III) catalyst, phenylsilane and dioxygen: acceleration of conjugate hydride reduction by dioxygen. Tetrahedron Lett. 41, 9725–9730. https://doi.org/https://doi.org/10.1016/S0040-4039(00)01727-5

Marenich, A. V, Cramer, C.J., Truhlar, D.G., 2009. Universal Solvation Model Based on Solute Electron Density and on a Continuum Model of the Solvent Defined by the Bulk Dielectric Constant and Atomic Surface Tensions. J. Phys. Chem. B 113, 6378–6396.

Marenich, A. V, Ho, J., Coote, M.L., Cramer, C.J., Truhlar, D.G., 2014. Computational electrochemistry : prediction of liquid-phase reduction potentials †. Phys. Chem. Chem. Phys. 16, 15068–15106. https://doi.org/10.1039/c4cp01572j

Mohan, N., Suresh, C.H., Kumar, A., Gadre, S.R., 2013. Molecular electrostatics for probing lone pair– p interactions. Phys. Chem. Chem. Phys. 15, 18401–18409. https://doi.org/10.1039/c3cp53379d

Namazian, M., Lin, C.Y., Coote, M.L., 2010. Benchmark Calculations of Absolute Reduction Potential of Ferricinium / Ferrocene Couple in Nonaqueous Solutions. J. Chem. theory Comput. 6, 2721–2725. https://doi.org/10.1021/ct1003252

Perera, I.R., Gupta, A., Xiang, W., Daeneke, T., Bach, U., Evans, R.A., Ohlin, C.A., Spiccia, L., 2014. Introducing manganese complexes as redox mediators for dye-sensitized solar cells. Phys. Chem. Chem. Phys. 16, 12021–12028. https://doi.org/10.1039/C3CP54894E

Politzer, P., Murray, J.S., 2002. The fundamental nature and role of the electrostatic potential in atoms and molecules. Theor. Chem. Acc. 108, 134–142. https://doi.org/10.1007/s00214-002-0363-9

Politzer, P., Murray, J.S., Peralta-Inga, Z., 2001. Molecular surface electrostatic potentials in relation to noncovalent interactions in biological systems. Int. J. Quantum Chem. 85, 676–684. https://doi.org/10.1002/qua.1706

R-Core-Team, 2018. The R Core Team: A language and enviroment for statistical computing.

Remya, G.S., Suresh, C.H., 2018. Assessment of the electron donor properties of substituted phenanthroline ligands in molybdenum carbonyl complexes using molecular electrostatic potentials. New J. Chem. 42, 3602–3608. https://doi.org/10.1039/C7NJ04592A

Remya, K., Suresh, C.H., 2016. Carbon rings: a DFT study on geometry, aromaticity, intermolecular carbon–carbon interactions and stability. R. Socienty Chem. Adv. 6, 44261–44271. https://doi.org/10.1039/c6ra06833b

Rillema, D.P., Jones, D.S., 1979. Structure of tris(2,2′-bipyridyl)ruthenium(II) hexafluorophosphate, [Ru(bipy)3][PF6]2; X-ray crystallographic determination. J. Chem. Soc. Chem. Commun. 849–851. https://doi.org/10.1039/C39790000849

Skyner, R.E., Mcdonagh, J.L., Groom, C.R., Mourik, T. Van, 2015. A review of methods for the calculation of solution free energies and the modelling of systems in solution. Phys. Chem. Chem. Phys. 17, 6174–6191. https://doi.org/10.1039/C5CP00288E

Sleightholme, A.E.S., Shinkle, A.A., Liu, Q., Li, Y., Monroe, C.W., Thompson, L.T., 2011. Non-aqueous manganese acetylacetonate electrolyte for redox flow batteries. J. Power Sources 196, 5742–5745. https://doi.org/https://doi.org/10.1016/j.jpowsour.2011.02.020

Sodhi, R.K., Paul, S., 2011. Nanosized Mn(acac)3 Anchored on Amino Functionalized Silica for the Selective Oxidative Synthesis of 2-arylbenzimidazoles, 2-arylbenzothiazoles and Aerobic Oxidation of Benzoins in Water. Catal. Letters 141, 608–615. https://doi.org/10.1007/s10562-010-0540-8

Sudo, A., Hirayama, S., Endo, T., 2010. Highly efficient catalysts-acetylacetonato complexes of transition metals in the 4th period for ring-opening polymerization of 1,3-benzoxazine. J. Polym. Sci. Part A Polym. Chem. 48, 479–484. https://doi.org/10.1002/pola.23810

Van Gorkum, R., Bouwman, E., Reedijk, J., 2004. Fast Autoxidation of Ethyl Linoleate Catalyzed by [Mn(acac)3] and Bipyridine: A Possible Drying Catalyst for Alkyd Paints. Inorg. Chem. 43, 2456–2458. https://doi.org/10.1021/ic0354217

Wang, Y.-F., Chiba, S., 2009. Mn(III)-Mediated Reactions of Cyclopropanols with Vinyl Azides: Synthesis of Pyridine and 2-Azabicyclo[3.3.1]non-2-en-1-ol Derivatives. J. Am. Chem. Soc. 131, 12570–12572. https://doi.org/10.1021/ja905110c

Yang, K., Bott, S.G., Richmond, M.G., 1993. Bidentate ligand substitution in PhCCo3(CO)9. Synthesis, molecular structure, and redox reactivity of PhCCo3(CO)7(cis-Ph2PCH□CHPPh2. J. Organomet. Chem. 454, 273–280. https://doi.org/https://doi.org/10.1016/0022-328X(93)83251-P

Zhao, Y., Truhlar, D.G., 2006. A new local density functional for main-group thermochemistry , transition metal bonding , thermochemical kinetics , and noncovalent interactions A new local density functional for main-group thermochemistry , transition metal bonding , thermochemical kin. J. Chem. Phys. 125, 194101. https://doi.org/10.1063/1.2370993

Supporting Information

Contents

FIGURE S1: RP(exp) vs RP(calc) and EA(calc)

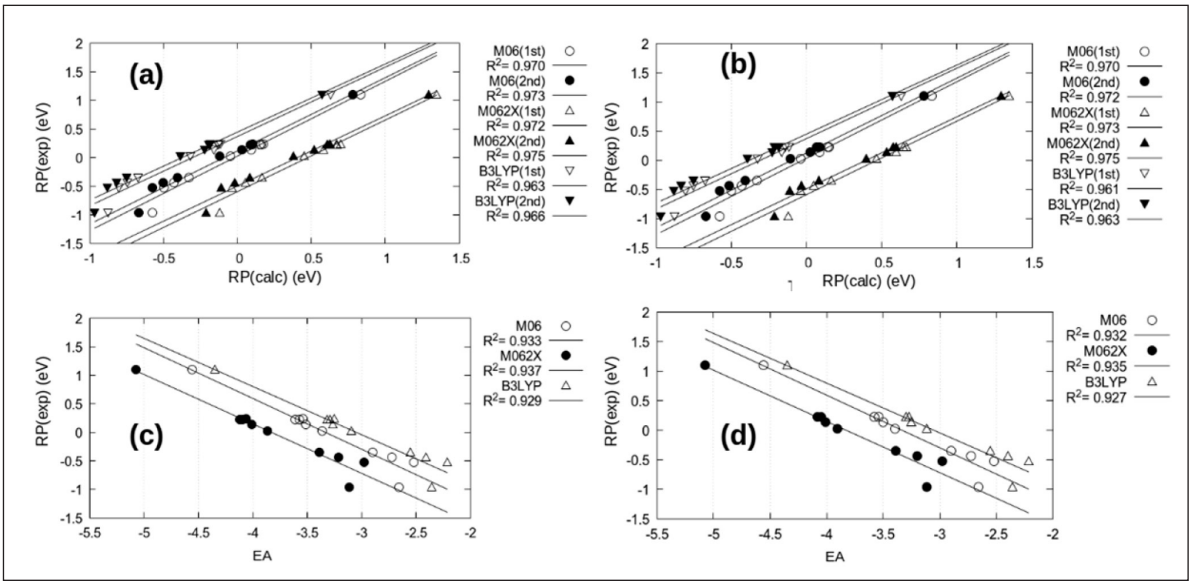

FIGURE S1: The correlation of the experimental reduction potential with the computed (a) reduction potential using the symmetrically substituted molecules and the *fac* isomers, (b) reduction potential using the symmetrically substituted molecules and the *mer* isomers, (c) electron affinity using the symmetrically substituted molecules and the *fac* isomers and (d) electron affinity using the symmetrically substituted molecules and the *mer* isomers. All reduction potentials are in V *vs* Fc/Fc^+.

FIGURE S2: IP(calc) ***vs*** EA(calc)

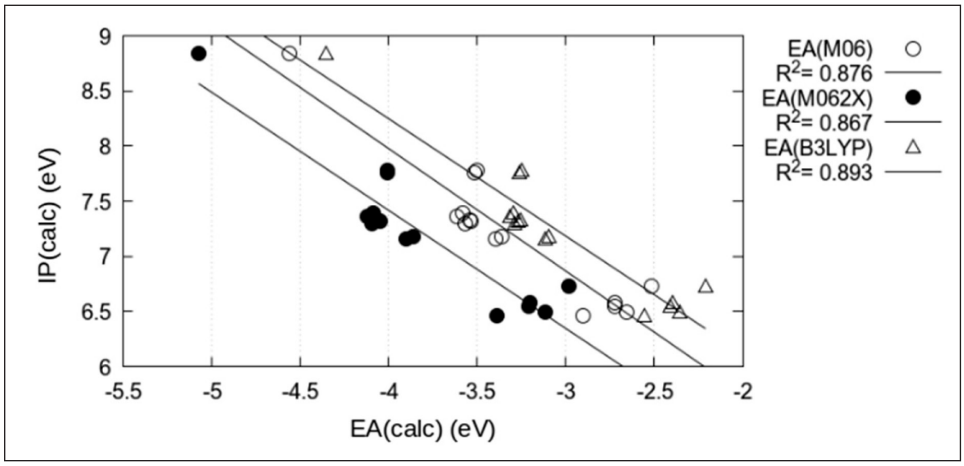

FIGURE S2: The correlation of the computed ionization potential using M06 with the computed electron affinities computed using M06, M062X and B3LYP.

TABLE S1: Energies

	E(B3LYP)	E(M06)	E(M062X)
1	-78762.70	-78740.45	-78753.60
2	-59505.27	-59494.23	-59500.97
3f	-75158.82	-75138.76	-75151.95
3m	-75158.83	-75138.77	-75151.95
4	-90812.37	-90783.28	-90802.92
5f	-83810.65	-83800.44	-83807.54
5m	-83810.68	-83800.46	-83807.55
6f	-125648.83	-125633.61	-125644.75
6m	-125648.86	-125633.65	-125644.80
7f	-99282.89	-99266.99	-99278.54
7m	-99282.93	-99267.02	-99278.56
8f	-99464.25	-99444.99	-99458.53
8m	-99464.29	-99445.04	-99458.56
9	-108115.54	-108106.17	-108113.62
10f	-91361.76	-91342.00	-91355.49
10m	-91361.75	-91341.98	-91355.46

TABLE S1: The energy (eV) of the neutral state of the complexes

TABLE S2: The parameters of the regression equation **Exp(RP) = b0 + b1X1** showing the level of correlation of the experimental reduction potential (Exp(RP)) with (a, b) the computed reduction potential using M06, M062X and B3LYP DFT functional, (c, d) electron affinity using M06, M062X and B3LYP DFT functional, (e,f) the change in MESP minimum (ΔV_{min}), and (g,h) electrostatic potential of Mn atom (ΔV_{Mn}), (i,j) the lowest (starts with l) and the highest (starts with h) electrostatic potential of the coordinating O atoms. Correlations are with the symmetrically substituted molecules and either the *fac* or *mer* isomers as indicated.

TABLE S2: Data analysis

X1	R2	b0	b1	RSE	t-value	Pr(>|t|)	F-statistic
"(a). Computed reduction potential (RP(calc)) using M06, M062X and B3LYP for symmetrical molecules and the *fac* isomers"							
E(M06-1st) *fac*	0.97	0.03	1.304	0.104	16.085	2.24E-07	258.7
E(M06-2nd) *fac*	0.973	0.12	1.277	0.099	16.943	1.49E-07	287
E(M062X-1st) *fac*	0.973	-0.591	1.25	0.099	16.81	1.59E-07	282.5
E(M062X-2nd) *fac*	0.975	-0.494	1.226	0.094	17.75	1.04E-07	315.1
E(B3LYP-1st) *fac*	0.963	0.372	1.21	0.116	14.344	5.45E-07	205.7
E(B3LYP-2nd) *fac*	0.966	0.449	1.188	0.111	14.99	3.87E-07	224.7
"(b). Computed reduction potential (RP(calc)) using M06, M062X and B3LYP for symmetrical molecules and the *mer* isomers"							
E(M06-1st) *mer*	0.97	0.035	1.31	0.11	15.009	1.40E-06	225.3
E(M06-2nd) *mer*	0.972	0.126	1.282	0.105	15.64	1.06E-06	244.6
E(M062X-1st) *mer*	0.973	-0.589	1.259	0.104	15.85	9.63E-07	251.3
E(M062X-2nd) *mer*	0.975	-0.489	1.233	0.1	16.5	7.33E-07	272.2
E(B3LYP-1st) *mer*	0.961	0.372	1.207	0.125	13.067	3.58E-06	170.7
E(B3LYP-2nd) *mer*	0.963	0.449	1.183	0.122	13.493	2.88E-06	182
"(c). Computed electronic affinity (EA) using M06, M062X and B3LYP for symmetrical molecules and the *fac* isomers"							
EA(M06) *fac*	0.933	-2.967	-0.89	0.155	-10.58	5.56E-06	112
EA(M062X) *fac*	0.938	-3.317	-0.866	0.15	-10.95	4.29E-06	119.9
EA(B3LYP) *fac*	0.929	-2.576	-0.845	0.16	-10.23	7.15E-06	104.7
"(d). Computed electronic affinity (EA) using M06, M062X and B3LYP for symmetrical molecules and the *mer* isomers"							
EA(M06) *mer*	0.932	-2.967	-0.89	0.165	-9.762	2.51E-05	95.29
EA(M062X) *mer*	0.935	-3.318	-0.867	0.161	-10.03	2.11E-05	100.5
EA(B3LYP) *mer*	0.928	-2.568	-0.841	0.17	-9.46	3.08E-05	89.5
(e). Change in MESP minimum (?Vmin) for the symmetrical molecules and the *fac* isomers of the neutral molecule and reduced molecule (*) where applicable							
ΔV_{min}(*fac*)	0.654	-0.158	0.031	0.307	3.634	8.36E-03	13.2
$\Delta^* V_{min}$(*fac*)	0.835	-0.402	0.034	0.212	5.955	5.67E-04	35.46
(f). Change in MESP minimum (ΔVmin) for the symmetrical molecules and *mer* isomers of the neutral molecule and reduced molecule (*) where applicable							
ΔV_{min}(*mer*)	0.804	-0.318	0.035	0.247	4.967	2.53E-03	24.67
$\Delta^* V_{min}$(*mer*)	0.922	-0.479	0.036	0.157	8.399	1.55E-04	70.54
(g). Change in electrostatic potential of Mn (ΔVMn) for the *fac* isomers of the neutral molecule and reduced molecule (*) where applicable							
ΔV_{Mn}(*fac*)	0.966	-0.45	14.074	0.097	14.052	2.19E-06	197.5
$\Delta^* V_{Mn}$(*fac*)	0.98	-0.594	14.873	0.073	18.62	3.20E-07	346.7
(h). Change in electrostatic potential of Mn (ΔVMn) for the symmetrical molecules and *mer* isomers of the neutral molecule and reduced molecule (*) where applicable							
ΔV_{Mn}(*mer*)	0.963	-0.457	13.911	0.108	12.44	1.65E-05	154.7
$\Delta^* V_{Mn}$(*mer*)	0.983	-0.602	14.99	0.074	18.36	1.68E-06	337.1
(i). Change electrostatic potential of two O atom (the one with lowest value (starts with l) and highest value (starts with h)) for the symmetrical molecules and the *fac* isomers of the neutral molecule and reduced molecule (*) where applicable							
Δ_{lVO}(*fac*)	0.925	-0.341	14.322	0.143	9.299	3.45E-05	86.47
Δ_{hVO}(*fac*)	0.927	-0.389	13.921	0.141	9.427	3.15E-05	88.88
Δ_{*lVO}(*fac*)	0.984	-0.489	15.892	0.066	20.7	1.54E-07	428.6
Δ_{*hVO}(*fac*)	0.968	-0.532	15.379	0.093	14.54	1.73E-06	211.5

TABLE S2: Data analysis *(continued)*

X1	R2	b0	b1	RSE	t-value	Pr(>|t|)	F-statistic
(j). Change in electrostatic potential of the two O atoms (the one with lowest value (starts with l) and highest value (starts with h)) for the symmetrical molecules and *mer* isomers of the neutral molecule and reduced molecule (*) where applicable							
Δ_{lvO}(*mer*)	0.939	-0.387	14.049	0.138	9.642	7.13E-05	92.96
Δ_{hvO}(*mer*)	0.931	-0.385	13.922	0.147	9.012	1.05E-04	81.21
Δ_{*lvO}(*mer*)	0.988	-0.494	15.781	0.062	22.06	5.67E-07	486.6
Δ_{*hvO}(*mer*)	0.966	-0.532	15.379	0.104	13.011	1.27E-05	169.3

Table S3: The computed values of the change in entropy (ΔS), gas phase free energy (ΔGgas), solvation energy ($\Delta\Delta G_{sol}$) and total reaction energy (ΔG_{rxt}) for the thermodynamic circle using DFT functional M06, M062X and B3LYP

TABLE S3: Thermodynamic parameters of reduction process

	ΔS	ΔG_{gas}	$\Delta\Delta G_{sol}$	ΔG_{rxt}(M06)	ΔG_{rxt}(M062X)	ΔG_{rxt}(B3LYP)
1	-6.26E-04	-0.280	-1.425	-4.363	-4.819	-4.064
2	-5.71E-04	-0.247	-1.673	-4.438	-4.899	-4.131
3f	-5.99E-04	-0.252	-1.528	-4.506	-4.990	-4.190
3m	-5.71E-04	-0.254	-1.529	-4.502	-4.983	-4.181
4	-6.53E-04	-0.274	-1.435	-4.609	-5.100	-4.262
5f	-5.17E-04	-0.217	-1.296	-5.028	-5.521	-4.778
5m	-5.44E-04	-0.225	-1.297	-5.022	-5.531	-4.772
6f	-5.99E-04	-0.242	-1.273	-5.084	-5.607	-4.803
6m	-6.53E-04	-0.260	-1.286	-5.084	-5.596	-4.817
7f	-5.99E-04	-0.250	-1.316	-5.106	-5.630	-4.820
8f	-5.71E-04	-0.233	-1.253	-5.100	-5.608	-4.805
8m	-5.71E-04	-0.241	-1.257	-5.079	-5.583	-4.796
9	-5.71E-04	-0.226	-0.988	-5.775	-6.288	-5.567
10f	-5.99E-04	-0.249	-1.272	-4.885	-5.386	-4.616
10m	-5.44E-04	-0.229	-1.270	-4.898	-5.404	-4.612